10th International Conference on Fracture Mechanics of Concrete and Concrete Structures
FraMCoS-10
J. Lemery, M. Ben Ftima and M. Leclerc
https://doi.org/10.21012/FC10.235472

EXPERIMENTAL INVESTIGATIONS ON THE SIZE EFFECT OF FRACTURE ENERGY FOR CONCRETES OF HYDRAULIC STRUCTURES

J. LEMERY[*], M. BEN FTIMA[†] AND M. LECLERC[††]

[*] École Polytechnique de Montréal, Montreal, CANADA
e-mail: joffrey.lemery@polymtl.ca

[†] École Polytechnique de Montréal, Montreal, CANADA
e-mail: mahdi.ben-ftima@polymtl.ca

[††] École Polytechnique de Montréal, Montreal, CANADA
e-mail: martin.leclerc@polymtl.ca

Keywords: Fracture process zone, Fracture energy, Size effect, Simplified Boundaries Effect Method, Mass concrete, experimental investigation.

Abstract: Numerical simulation using non-linear constitutive laws turns out to be a necessity for the case of hydraulic structures affected by the alkali-aggregate reaction (AAR). The fracture energy constitutes an important input parameter for these nonlinear laws and requires an experimental characterization step. Because of the size of the hydraulic structures, it is a question here of characterizing a representative fracture energy and independently of all size effects phenomena.

As such, this work aims to characterize the asymptotic fracture energy of two different mixtures of an existing hydraulic facility, having maximum aggregate sizes of 38 mm and 76 mm. It constitutes a first phase of a project whose final objective is to characterize the impact of the AAR on the asymptotic fracture energy.

The experimental campaign consists of 71 specimens divided between two mixtures with different maximum aggregate sizes: 38 and 76 mm and two different compositions: without and with alkali overdose. 29 of the 71 specimens were already tested on two different experimental setups: a three-point bending test (RILEM TPB) and a wedge splitting test (WST). In order to filter the size effects, the method known as SBEM for Simplified Boundary Effect Method was used [1], based on a bilinear distribution of local fracture energy due to a boundary effect.

The analysis of the results of the specimens tested confirms the presence of the size effect for the tested mixtures and the positive impact of the maximum aggregate size on the fracture energy. The results show that the fracture energy from a given test is proportional to the area of the cracked concrete surface. It was possible to extract, using the SBEM method, an asymptotic fracture energy independent of the size of the specimens and which would represent the fracture energy of a RILEM TPB test or a WST test on a very large specimen. This asymptotic fracture energy has a magnitude of an order of 2 to 3 times greater than that obtained from a TPB RILEM test, or that predicted by the semi- empirical equations based on this standardized test.

1 INTRODUCTION

The safe management of hydraulic facilities (dams, spillways ...) is a challenging task for owners and requires the development of predictive simulation tools in order to assess safety and sustainability of these infrastructures. In this context, the evolution of concrete properties over time shall be considered in order to provide valuable inputs to the sophisticated concrete constitutive laws used in the simulations. Seasonal temperature variations and wetting and drying cycles can be considered as natural environmental conditions that contribute to the degradation of concrete properties. Additionally, this degradation can be accelerated due to the presence of alkali-aggregate reaction pathology (AAR) which is an acid-base chemical reaction known to occur in concrete for certain types of aggregates and under certain moisture and temperature conditions. Structural manifestation of this reaction is due to the expansive nature of the alkali-silica gel, product of this reaction, when it comes in contact with moisture. This internal expansion generally leads to micro-cracking, loss of strength and stiffness at the material level.

Numerical simulation using non-linear constitutive laws turns out to be a necessity for the case of hydraulic facilities affected by AAR. These models use generally a complete 3D discretization of the geometry and are based on concrete constitutive laws allowing to model concrete cracking and the different complex physico-chemical interactions that may take place. For the specific case of hydraulic structures, which are massive and generally lightly reinforced/un-reinforced concrete structures, the post-cracking energy of concrete is a very important input parameter. This energy, often called fracture energy in the literature and noted G_F, has a significant impact on simulation results due to the large fractured areas that can be involved (Figure 1). This work is part of a large university/industry collaboration project whose objective is the characterization of the fracture energy for an existing hydraulic facility affected by AAR.

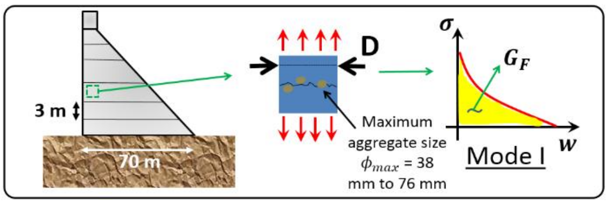

Figure 1: Fracture energy and typical dimensions of a concrete hydraulic dam

The proper characterization of G_F for existing hydraulic structures faces two major difficulties. The first one is related to the known dependency of this parameter on the specimen size, or size effect, a phenomena that has been experimentally proven in the last century. Figure 2 [3] shows experimental results of wedge splitting tests related to concrete with large aggregate sizes and shows the dependency of the fracture energy on the nominal size *D* of tested specimens. The figure shows also an asymptotic trend towards a value of fracture energy quasi-independent of specimen size. This asymptotic value, noted $G_{F\infty}$ in this work, is independent of all scale phenomena and actually represents the fracture energy measured on a very large specimen. It is also the value that shall be used for the specific context of hydraulic structures. The second difficulty is related to the large aggregates used in this industry which makes questionable the characterization results based on concrete cores that can be extracted from the facility (typically *D* is less than 300 mm in Figure 1).

To overcome the second difficulty, a reconstitution of concrete was considered while attempting to reproduce as much as possible the physical and chemical properties of the original concrete used for construction. Reconstituted concrete is made from the original aggregate unaltered with the AAR. Two types of concrete mixtures were used for the construction of the main dam, a 1 1/2 "mixture ($\phi_{max} = 38\,mm$) and a 3" mixture

($\phi_{max} = 76\ mm$). Since larger aggregates came from the crushing of the excavation rock, it was possible to extract from the site, pieces of rock having the same characteristics as the coarse aggregates used in the original mix. To accelerate the AAR reaction in a controlled humidity/temperature room, the cement of some of the mixtures (called reactive in this work) were overdosed in alkali to a value of 1,25 % of the cement mass (Na_2O equivalent). The other portion of the mixes (called non-reactive in this work) were made using the original alkali content of 0,54%.

To overcome the size dependency difficulty, wedge splitting test (WST) is used in conjunction with the method known as SBEM for Simplified Boundary Effect Method [1]. The conventional RILEM three-point bending test (RILEM TPB) is also used for comparison purposes. Digital image correlation (DIC) and Acoustic emission (AE) techniques were used to monitor the tests, additionally to the traditional instrumentation.

The experimental campaign consists of 71 specimens divided between two mixtures with different maximum aggregate sizes: 38 and 76 mm and two different compositions: without (non-reactive) and with alkali overdose (reactive). 29 of the 71 specimens were already tested and only the results of the non-reactive mixtures are considered in this paper with a special emphasis on the size effect phenomenon.

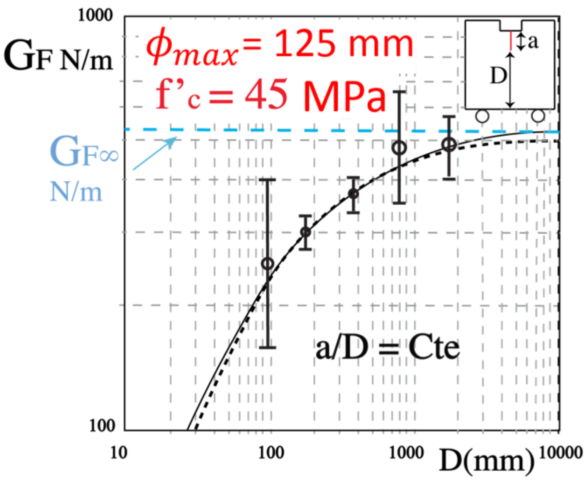

Figure 2: Size effect on fracture energy (Adapted from [3])

2 THEORICAL BACKGROUND

Concrete is a heterogenous material with a complex behavior that cannot be modeled directly using the linear elastic fracture mechanics (LEFM). Non-linear fracture mechanics (NLFM) can be alternatively used and considers a zone of nonlinearity of a finite size at the tip of the crack, known as the fracture process zone (FPZ).

2.2 Fictitious crack model

Many toughening mechanisms contribute to energy dissipation within the FPZ [4]: aggregate bridging, surface roughness, crack branching,… All these mechanisms allow force transmission and can be modeled by cohesive pressures acting on the crack surfaces as shown in Figure 3. This pressure is equal to zero at the notch tip, and to the tensile strength of concrete at the end of the FPZ. For the crack propagation, the energy release provided by the load Q, noted G_Q has to reach a critical value matching on the one hand the energy necessary for the creation of new cracked surfaces as described by the LEFM mode I, noted G_{Ic}, plus on the other hand the energy to break the cohesive pressures, noted G_σ, following the equation:

$$G_Q = G_{Ic} + G_\sigma = G_{Ic} + \int_0^{w_t} \sigma(w)dw \qquad (1)$$

where w_t is the opening at the crack tip as shown in Figure 3, and *σ(w)* describes the cohesive stress-crack opening curve.

In the fictitious crack approach introduced by Hillerborg [5, 6], the energy to create new surfaces (G_{Ic}) is assumed small compared to that required to separate them (G_σ), hence $G_Q \approx G_\sigma$ in Eq. 1. Hillerborg introduced the fracture energy as a material property, and as the energy required to overcome the cohesive pressure, or the area under the entire stress-crack opening curve as shown in Figure 3. Thus, the fracture energy G_F is defined by the following equation

$$G_F = \int_0^{w_c} \sigma(w)dw \qquad (2)$$

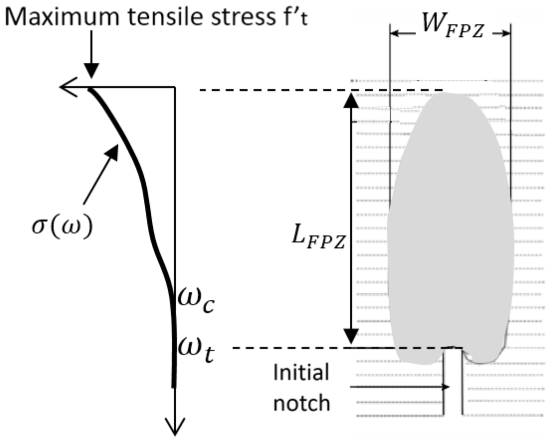

Figure 3: FPZ model decomposed into segments and stresses cracking distribution (Modified from [7])

2.3 Experimental determination of fracture energy

WST test [8] and RILEM TPB [6] are two suggested experimental tests to characterize the fracture energy of a given concrete mixture. In both tests, the fracture energy G_{F_EXP} is measured as the *average* energy given by dividing the total fracture work by the projected cracked area.

$$G_{F\_EXP} = \frac{1}{(D-a)B}\int P d\delta \qquad (3)$$

Where *B* is the thickness of the specimen, *D* is the depth of the specimen and ***a*** is the length of the initial notch. Hence *D* - *a* is the length of the fractured ligament. According to the experimental evidence of Figure 3, we can write the following equation :

$$\lim_{D-a\to\infty} G_{F\_EXP} = G_{F\infty} \qquad (4)$$

Hence, the only case where the fracture energy can be considered as a material property is the case where the ligament length is infinitely large with respect to the size of FPZ, which is the case for typical elements of hydraulic structures (Figure 1). Many theories tried to give an interpretation to this phenomenon, among them the boundaries effect theory ([7],[9]) considered in this work.

2.2 Boundaries Effect theory

According to this theory, as the crack approaches the back boundary of the specimen, the size of the FPZ diminishes in terms of width W_{FPZ} and length L_{FPZ}. Consequently, the cohesive stress field get narrower and the fracture energy described by Eq. 3 becomes location dependent $\boldsymbol{G_F(x)}$. Hu and Wittman [10] introduced the local fracture energy related to the stress-crack opening curve, and which follows a bi-linear variation $\boldsymbol{g_f(x)}$. This bilinear function represented in Figure 4 consists of a horizontal asymptote which starts to decrease to zero from a distance $\boldsymbol{a_1}$ from the back boundary. The asymptotic value $G_{F\infty}$ corresponds therefore to the horizontal portion of the local fracture energy.

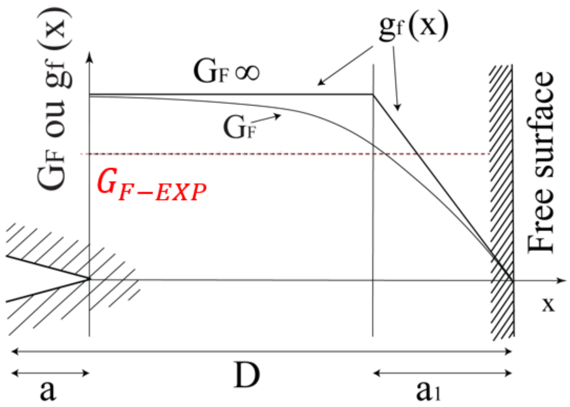

Figure 4: Boundaries effect theory (Modified from [7])

AE acquisition has been performed during crack propagation by Muralidhara et al. [11] to confirm this theory. Results were relevant with this theory and highlighted a trilinear variation of the local fracture energy. However, the rising time of the FPZ was so short that a bilinear approximation was considered adequate. Duan et al. [7] established the boundary effect model where the size dependency of experimental results from the

RILEM equation is due to an artificial reduce of the average calculated value induced by the decreasing local fracture energy near of the back boundary. Thus, the expression relating specific fracture energy G_F and the asymptotic size-independent value $G_{F\infty}$ are:

$$G_F\left(\frac{a}{D}\right) = \frac{\int_0^{D-a} g_f(x)dx}{D-a} = \begin{cases} G_{F\infty}\left[1-\dfrac{1-a_1/D}{2(1-a/D)}\right] & si \quad 1-a/D > a_1/D \\ \dfrac{G_{F\infty}}{2}\dfrac{(1-a/D)}{a_1/D} & si \quad 1-a/D \leq a_1/D \end{cases} \tag{5}$$

Since the free-border effect comes from the presence of free boundaries, the thickness of the specimen may also have an influence on the size of FPZ. This effect has been studied by Duan et al. [12] and the authors have shown that this effect is negligible for specimens with a thickness larger than 4 times the maximum aggregate size.

Finally, Abdalla and Karihaloo [13] introduced the Simplified Boundaries Effect Method (SBEM) as a simplified method to estimate the parameters of the bilinear curve ($G_{F\infty}$ and a_1), by conducting two sets of WST tests, using two different ratios of a/D. Identification of $G_{F\infty}$ and a_1 can therefore be done using Eq. 5.

3 EXPERIMENTAL PROGRAM

The full experimental campaign consists of 71 concrete specimens mainly divided between two mixtures with two different maximum aggregate sizes 38 mm and 76 mm (Table 1).

WST specimens with 38 mm aggregate are 300 mm (*H*) * 300 mm (*L*) * 200 mm (*B*), and specimens with 76 mm aggregate are 600 mm (*H*) * 600 mm (*L*) * 400 mm (*B*) (Figure 5). For each mixture, cements without alkali overdose (noted type A) and with alkali overdose (noted type B) were used. Two different a/D ratios were considered in this work: a/D = 0,1 (noted WS01) and a/D = 0,5 (noted WS05).

RILEM TPB specimens were considered only for the 38 mm aggregate mixtures with dimensions 1450 mm (*L*) * 300 mm (*D*) * 150 mm (*B*) (Figure 6). Type B specimens were stored in a controlled temperature/humidity chamber to accelerate the chemical AAR and are planned to be tested at different advancements ζ of the AAR reaction as shown in Table 1. Only type A specimens and B specimens with 0% advancement of AAR ($\xi = 0\%$) were tested and are presented in this paper.

Table 1: Experimental program for the full project

Experimental Protocol						
Ident.	Mixture	Test type	Dimensions (mm)	Replications	ζ	a/D
A-38-WS01	38 mm	WS	300x300 x200	4	0%	0.1
A-38-WS05	38 mm	WS	300x300 x200	3	0%	0.5
A-38-TPB	38 mm	TPB	300x150 x1450	3	0%	0.5
A-38-CAR	38 mm	CAR	D150x300	6	0%	-
A-76-WS01	76 mm	WS	600x600 x400	4	0%	0.1
A-76-WS05	76 mm	WS	600x600 x400	3	0%	0.5
A-76-CAR	76 mm	CAR	D150x300	6	0%	-
B-38-WS01	38 mm	RAG + WS	300x300 x200	3 (x4)	0%-20%-60%-80%	0.1
B-38-WS05	38 mm	RAG + WS	300x300 x200	3 (x4)	0%-20%-60%-80%	0.5
B-38-WS01-c*	38 mm	RAG + WS	300x300 x200	3 (x2)	20%-80%	0.1
B-38-WS05-c*	38 mm	RAG + WS	300x300 x200	3 (x2)	20%-80%	0.5
B-38-CAR	38 mm	RAG + WS	D150x300	6 (x4)	0%-20%-60%-80%	-
B-76-WS01	76 mm	RAG + WS	600x600 x400	3 (x3)	0%-30%-70%	0.1
B-76-WS05	76 mm	RAG + WS	600x600 x400	3 (x3)	0%-30%-70%	0.5
B-76-CAR	76 mm	RAG + WS	D150x300	6 (x4)	0%-30%-70%	-

The specimens with a c* designation in their name (Example: B-38-WS01-c*) were cast on the side to assess the influence of pouring direction on fracture energy. Finally, specimens for the characterization of the mixture properties were also considered (noted CAR in Table 1).

3.1 The Wedge Splitting Test

As mentioned above, most of the testing has been carried out with the WST. This test is an advanced version of the 3-point bending test where the experimenter simply uses the "central part" of the beam. The splitting forces *Ps* are generated from the vertical force of the hydraulic jack *Pv* through a wedge/rollers mechanism as described in Figure 5. If frictional effects are neglected, *Ps* can be deduced from *Pv* using the following equation in which $\emptyset$ is the inclination angle of the wedge:

$$P_S = \frac{P_v}{2\tan(\phi)} \quad (6)$$

In comparison with the original version of the WST [8], two support rollers were considered at the bottom of the specimen and are aligned with centers of gravity of each half block at the right and at the left of the notch. This ensures a more stable crack propagation, a zero work contribution of the self-weight of specimen during the test and avoids multi-axial distribution of the stresses at the end of the test ([14]).

The tests were driven in a closed-loop servo-hydraulic dynamic testing machine and at a CMOD opening slow rate of 0,0005 mm/s. For all the tests, the same wedge angle $\emptyset = 15°$ is used.

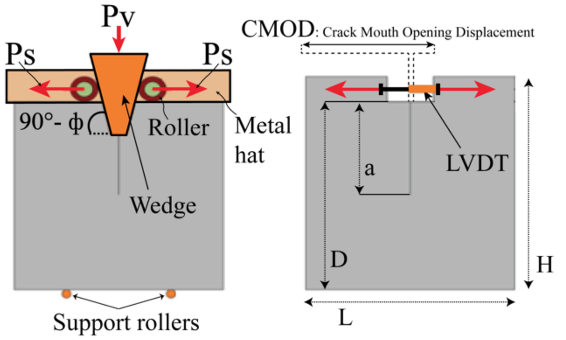

Figure 5: WST Test

3.2 The TPB RILEM Test

The configuration of the TPB RILEM test is shown in Figure 6. Since the RILEM 50-FMC does not give a strict numerical indication of the loading rate, we consider orders of magnitude for the opening of the CMOD present in the literature between 0.003 mm / min and 0.06 mm / min, and choose a CMOD of 0.005mm / min.

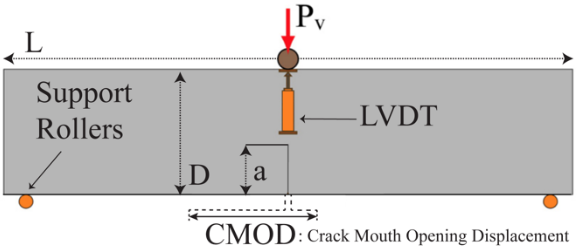

Figure 6: TPBT Test

3.3 Monitoring equipment

Several instrumentations were used to monitor the WST tests during the fracturing process.

LVDTs

Linear Variable Differential Transformer were mounted on different parts of specimens. Two LVDT of 0,002 mm of accuracy were placed on top of the wedge corners as shown in Figure 7 and were used to control the WST tests. Other LVDTs were placed at the level of the roller axis (Figure 5) in order to monitor the CMOD all along the test. LVDTs were also mounted between the rollers supports to quantify energy dissipation through friction.

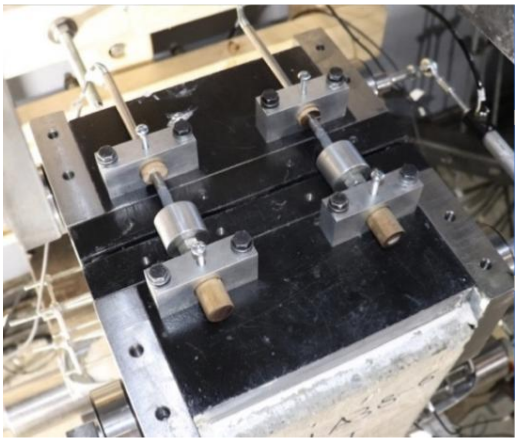

Figure 7: Upper LVDT picture

DIC Monitoring

Digital Image Correlation is a non-disturbing and non-contact measuring technique used to monitor the displacement field using a system of cameras, points on the surface of the specimen and a data post-processing software. This technique provides richer data than gauge-based measurement techniques as images of the entire surface of the specimen are recorded, and then processed conveniently after the test. In our experiments, only one of the two side faces of the WST was monitored using DIC (Figure 8).

Figure 8: Painting tools for DIC and example of surface preparation

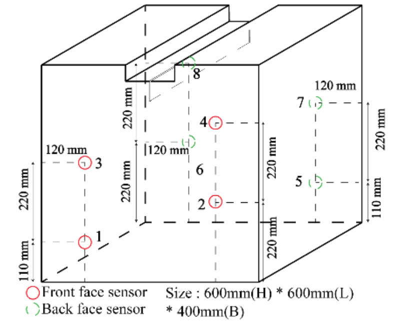

Figure 10: AE position sensors for A76 specimens

Horizontal load, kN

AE Monitoring

The AE equipment used for this campaign was from Vallen Acoustic Emission. Eight sensors with a 150 kHz resonance frequency were used and were placed according to the Figures 9-10.

Sensors were positioned on the non-painted DIC side face of each specimen. For a better fixation of the sensors on the concrete surface, special tripods were designed and manufactured as shown in Figure 11. They allow to maintain the sensor, with a fixed force of 14 N as required by sensors supplier. Finally, the surfaces were cleaned, and silicon grease was used to ensure a good transfer of elastic waves between specimens and sensors. Noise test were performed before every test to check that the laboratory noise stays under 30 dB. A fixed threshold of 40 dB for signal detection was used.

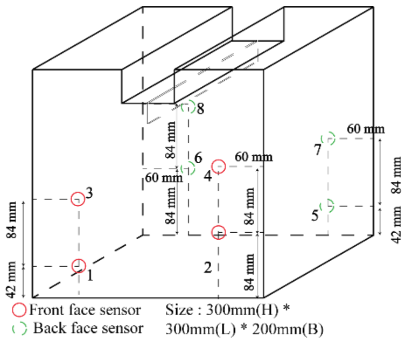

Figure 9: AE position sensors for A38 specimens

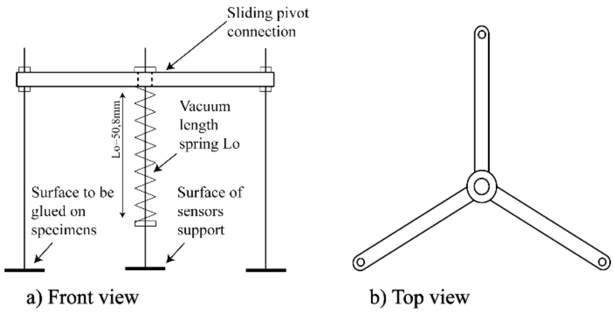

Figure 11: Tripods used for fixation of acoustic sensors

4 RESULTS AND DISCUSSION

4.1 Material testing

Table 2 gives the results of the characterization tests conducted for each concrete mixture.

Table 2: Characterization tests

Ident.	Aggr. size	Time since casting	Comp. strength f'c	c.o.v f'c	Elasticity modulus	Poisson's coef.	Splitting tensile strength
-	mm	Days	f'c (MPa)	%	(MPa)	v	f_{sp} (MPa)
A38	38	84	20,3	3,3 %	25434	0,27	1,71
A76	76	175	25,4	3,2 %	35937	0,28	-

4.2 WST tests

Figures 12 and 13 present the load-displacement curves of A38 and A76 specimens. In general, a quite good repeatability can be observed for peak strengths and also for post-peak curves. The A76-WS05-3 load/displacement curve presented a drop due to the presence of a large aggregate in the cracking path near a CMOD displacement of 7 mm, as shown in figure 13.

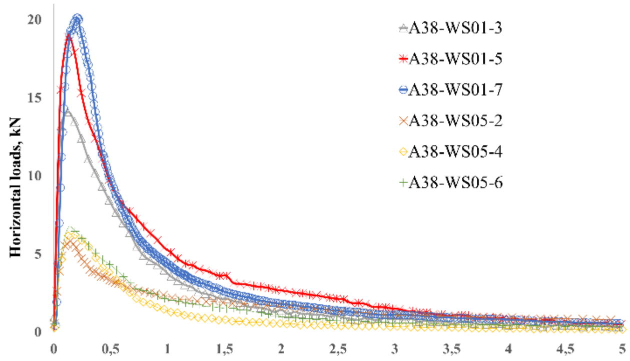

Figure 12: Results for WST of A38 specimens

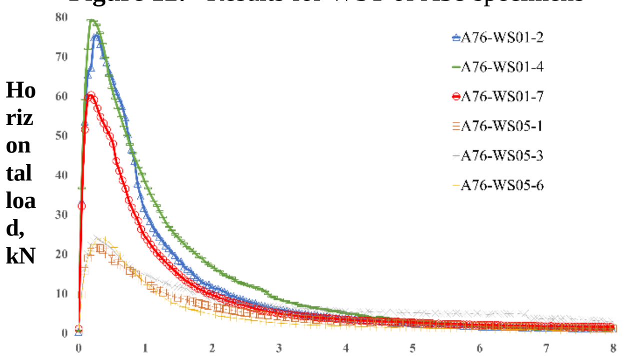

Figure 13: Results for WST of A76 specimens

4.3 Computation of fracture energy G_F

Tables 3 shows the computed fracture energies from the load/CMOD curves. The G_F values obtained from the RILEM TPB test are lower than those obtained from the WST test. Also, the G_F values obtained from WST with ratios a/D = 0,5 are lower than those obtained from WST with ratios a/D =0,5. As it will be shown later, these results are due the different cracked areas between these tests.

Table 1: RILEM fracture energy for similar specimens with corresponding SBEM fracture energy

Type	Average G_F	c.o.v of G_F	$G_F\infty$	a_1
-	N/m	-	N/m	mm
A38-TPB	184	10%	-	-
A38-WST a/D =0,5	306	33%	470	99
A38 -WST a/D =0,1	370	13%		
A76-WST a/D =0,5	422	13%	669	220
A76-WST a/D =0,1	521	13%		
B76-WST a/D =0,5	448	13%	636	197
B76-WST a/D =0,1	511	26%		

As anticipated, the computed fracture energy increases with the size of maximum aggregate. Finally, the results of the B76 mixture tested at $\xi = 0\%$ advancement, if compared to the A76 results, show that overdose in alkali had a little influence of fracture properties of concrete. This validates the feasibility and the consistency of the full project aiming to characterize the influence of the AAR advancement on the fracture properties of concrete.

4.4 SBEM resolution and asymptotic fracture energy $G_{F\infty}$

Using the SBEM method and Eq. 5 presented earlier, values of a_1 and the asymptotic fracture energy $G_{F\infty}$ were computed for each mixture. The results are presented in Table 3. If comparing the a_1 values for different mixtures, the boundary effect appear to be proportional to the maximum aggregate size which is a quite interesting result. Also, the computed asymptotic fracture energy is 2,5 times higher than the value obtained from the TPB RILEM test (for A38) and 1,5 times higher than values obtained from WST tests with small fractured areas (a/D = 0,5). These results are consistent with those obtained in previous studies and shown in Figure 2. The computed $G_{F\infty}$ values in this work are consistent with values found in other works ([1], [12] and [15]).

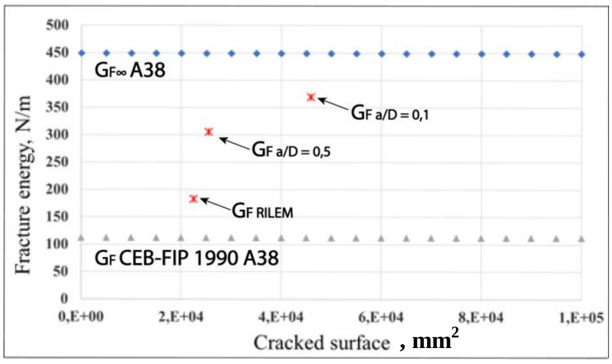

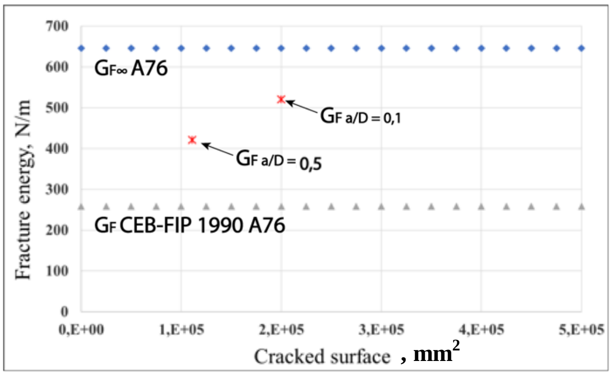

Figure 14: Fractures energies for both mixtures versus cracked surface

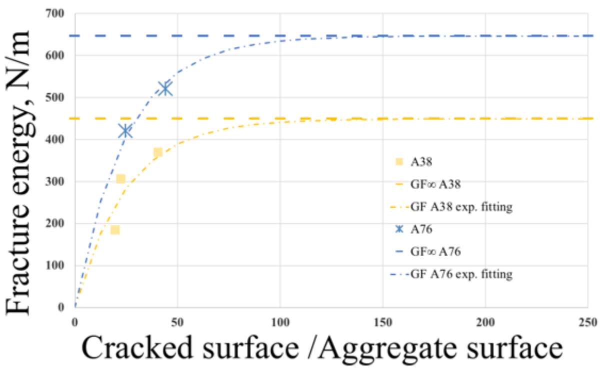

Figure 15: Fracture energy versus the cracked surface / aggregate surface ratio

Figure 14 presents the different assessed fracture energies versus the cracked ligament area. It clearly shows the dependency of the fracture energy $\boldsymbol{G_F}$ on the cracked area and also shows an asymptotic tendency towards the value of $\boldsymbol{G_{F\infty}}$ for each mixture. The fracture energy estimated by the TPB RILEM is the lowest, and as anticipated it is the closest to the value computed from the semi-empirical equation of the CEB-FIP 90 model code.

In Figure 15, the assessed fracture energies of both mixtures are represented according to the ratio $\boldsymbol{r}$ of the cracked area over the nominal maximum aggregate area $(\frac{\pi\Phi_{max}^2}{4})$. Again, an asymptotic tendency can be noticed. The following equation was found to better fit with both mixtures (see exponential curves in Figure 15):

$$G_F = G_{F\infty} * (1 - e^{-\frac{r}{25}}) \tag{7}$$

which means that the fracture energy would reach 90 % of the asymptotic fracture enrgy for a surface ratio equal to $\boldsymbol{r}$ = 3*25 = 75.

5 AE RESULTS

Figure 16 represents the normalized cumulative energies extracted from acoustic acquisition versus the normalized CMOD. At each recorded microcracking event, the acoustic energy captured at the nearest sensor is stored. All cumulative energies in Figure 16 are normalized with respect to their asymptotic values at the end of the tests. The CMOD curves are also normalized with respect to their values at the end of the tests. It is interesting to note two different tendencies in Figure 16, each one is related to a ratio a/d ratio no matter the mixture. For the specimens with short initial notches $(\frac{a}{d} = 0{,}1)$, the normalized cumulative energies appear to converge more rapidly to their asymptotic values. A possible interpretation of this effect is that the FPZ is less disturbed by the boundary effects when the fractured surface is large, therefore, it reaches its asymptotic size right at the beginning of the test.

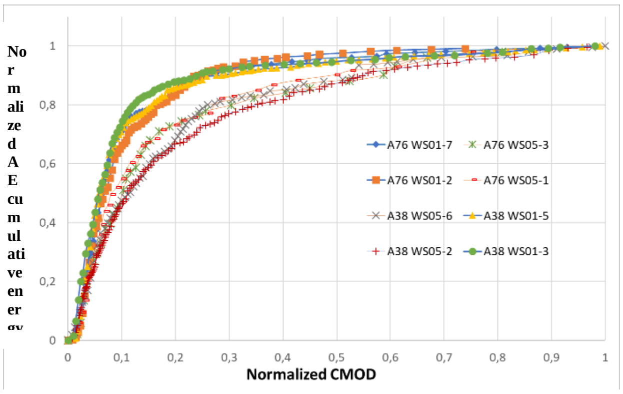

Figure 16: Normalized AE cumulative energy versus normalized CMOD for all type A specimens

6 CONCLUSIONS

From the above results and discussions, the following conclusions can be drawn:

- The testing experimental protocol of WST specimens offered stable, robust and repeatable tests for large sizes of aggregates used in hydraulic structures.
- For both 38 mm and 76 mm mixtures, the assessed fracture energies exhibited a dependency on the length of the fractured ligament or on the fractured surface. The TPB RILEM gives a lower bound value of the fracture energy.
- Using the SBEM method, it was possible to compute an asymptotic fracture energy which is believed to be independent of the specimen size and is 2,5 times higher than the one assessed by the TPB RILEM test. This value of asymptotic fracture energy shall be used in the FE analyses of hydraulic structures due to the very large sizes of the members used in this field.
- The parameter a_1 related to the depth of the boundary effect in the bilinear model, was found to be proportional to the maximum aggregate size used in the concrete mixture.
- The comparison between assessed G_F and $G_{F\infty}$ values suggests that the size-independent fracture energy could be obtained with specimens with cracked surfaces much larger than the nominal maximum aggregate surface (x 75), and with a cracked ligament 6 to 9 times larger than the size of the maximum aggregate used in the mixture.
- Using AE, it was possible to highlight two different tendencies of the evolution of the cumulative acoustic energies. In the tests with low a/D values and hence with larger fractured surfaces, the FPZ reaches rapidly its asymptotic size since it is less disturbed by the boundaries effects.

ACKOWLEDGMENT

The authors would like to acknowledge the financial support of the Natural Sciences and Engineering Research Council of Canada and Hydro-Quebec.

REFERENCES

1. Karihaloo, B.L., H. Abdalla, and T. Imjai, *A simple method for determining the true specific fracture energy of concrete.* Magazine of concrete research, 2003. **55**(5): p. 471-481.
2. Hu, X. and K. Duan, *Influence of fracture process zone height on fracture energy of concrete.* Cement and concrete research, 2004. **34**(8): p. 1321-1330.
3. Trunk, B. and F. Wittmann, *Influence of size on fracture energy of concrete.* Materials and Structures, 2001. **34**(5): p. 260-265.
4. Shah, S.P., S.E. Swartz, and C. Ouyang, *Fracture mechanics of concrete.* John Willy & Sons Inc, New York, 1995.
5. Hillerborg, A., *Analysis of one single crack.* Fracture Mechanics of Concrete (Developments in civil engineering), 1983: p. 223-249.
6. Hilleborg, A., *The theoretical basis of a method to determine the fracture energy of concrete.* Materials and structures, 1985. **18**: p. 291-296.
7. Duan, K., X.-Z. Hu, and F. Wittmann, *Explanation of size effect in concrete fracture using non-uniform energy distribution.* Materials and Structures, 2002. **35**(6): p. 326.
8. Brühwiler, E. and F. Wittmann, *The wedge splitting test, a new method of performing stable fracture mechanics tests.* Engineering fracture mechanics, 1990. **35**(1-3): p. 117-125.
9. Hu, X. and F. Wittmann, *Size effect on toughness induced by crack close to free surface.* Engineering fracture mechanics, 2000. **65**(2): p. 209-221.
10. Hu, X.-Z. and F. Wittmann, *Fracture energy and fracture process zone.* Materials and Structures, 1992. **25**(6): p. 319-326.

11. Muralidhara, S., B.K. Raghu Prasad, H. Eskandari, and B.L. Karihaloo, *Fracture process zone size and true fracture energy of concrete using acoustic emission.* Construction and Building Materials, 2010. **24**(4): p. 479-486.
12. Duan, K., X.-Z. Hu, and F.H. Wittmann, *Thickness effect on fracture energy of cementitious materials.* Cement and concrete research, 2003. **33**(4): p. 499-507.
13. Abdalla, H. and B.L. Karihaloo, *Determination of size-independent specific fracture energy of concrete from three point-bend and wedge splitting tests.* Magazine of concrete research, 2003. **55**(2): p. 133-141.
14. Trunk, B., G. Schober, H.K. Helbling, , and F.H. Wittman , *Fracture mechanics parameters of autoclaved aerated concrete.* Cement and Concrete Research, 1999. **29**(6): p. 855-859.
15. Zhao, Z., S.H. Kwon, and S.P. Shah, *Effect of specimen size on fracture energy and softening curve of concrete: Part I. Experiments and fracture energy*. Cement and Concrete Research, 2008. **38**(8): p. 1049-1060.
16. Saliba, J., M. Matallah, A. Loukili, J.P. Regoin, D. Grégoire, L. Verdon, and G. Pijaudier-Cabot, *Experimental analysis of crack evolution in concrete by the acoustic emission technique.* Frattura ed Integrità Strutturale, 2015. **9**(34).